Simulations of a Heat-Wave Event in New York City Using a Multilayer Urban Parameterization

ESTATIO GUTIÉRREZ AND JORGE E. GONZÁLEZ

Mechanical Engineering Department, City College of New York, New York, New York

ALBERTO MARTILLI

Centro de Investigaciones Energéticas, Medioambientales y Tecnológicas, Madrid, Spain

ROBERT BORNSTEIN

Meteorology Department, San Jose State University, San Jose, California

MARK AREND

NOAA-Cooperative Remote Sensing Science and Technology Center, City College of New York, New York, New York

(Manuscript received 24 January 2014, in final form 15 September 2014)

ABSTRACT

The Weather Research and Forecasting mesoscale model coupled to a multilayer urban canopy parameterization was used to evaluate the evolution of a 3-day heat wave in New York City, New York, during the summer of 2010. Results from three simulations with different degrees of urban modeling complexity and one with an absence of urban surfaces are compared with observations. To improve the city morphology representation, building information was assimilated and the land cover land-use classification was modified. The thermal and drag effects of buildings represented in the multilayer urban canopy model improve simulations over urban regions, giving better estimates of the surface temperature and wind speed. The accuracy of the simulation is further assessed against more simplified urban parameterizations models. The nighttime excessive cooling shown by the Building Energy Parameterization is compensated for when the Building Energy Model is activated. The turbulent kinetic energy is vertically distributed when using the multilayer scheme with a maximum at the average building height, whereas turbulence production is confined to a few meters above the surface when using the simplified scheme. Evidence for the existence of horizontal roll vortices is presented, and the impact that the horizontal resolution and the time step value have on their formation is assessed.

1. Introduction

A heat wave is a prolonged period of temperatures considered to be abnormally high for a particular area. They are associated with high pressure circulation patterns that produce subsidence, light winds, clear skies, and warm air advection. Heat waves vary across regions in their intensity, duration, and timing. Meehl and Tebaldi (2004) examined the future behavior of the heat waves using a global coupled climate model. Assuming a scenario with poor policy intervention to mitigate greenhouse gases, the model indicated a heat-wave severity anomaly greater than 3°C in the western and southern United States while the northeast part of the country would experience anomalies of 2°C. A general increase of nighttime minima is also expected. These projections reflect the need for a better understanding of extreme heat events in highly populated urban environments.

Urban heat island (UHI) effects could intensify the magnitude of a heat wave. Vegetation substitution by pavement and concrete structures has a substantial impact on surface conditions and the vertical configuration

Denotes Open Access content.

Corresponding author address: Estatio Gutiérrez, Dept. of Mechanical Engineering, City College of New York, 260 Convent Ave., Apt. 96, New York, NY 10031.
E-mail: estatio@yahoo.com

DOI: 10.1175/JAMC-D-14-0028.1

© 2015 American Meteorological Society

of the lower atmosphere. Changes in physical characteristics of the surface such as albedo, thermal capacity, and heat conductivity retard the nocturnal cooling of urban surfaces between sunset and midnight when rural areas are cooling more rapidly (Oke and Bornstein 1981). This effect is enhanced by the decrease of surface moisture availability, changes in radiative fluxes, and surface flow due to the complex geometry of streets and tall buildings as well as anthropogenic heat release. Periods of heat stress could have negative repercussions for human health. The higher the temperature or the longer the heat wave, the more work is required by the cardiovascular system to maintain a normal body temperature; therefore, more intense or longer heat waves are likely to have greater health effects (Anderson and Bell 2011). Two well-documented examples in the Northeast are the 1966 heat wave that produced 1181 deaths (Schuman 1972) and the 1995 Chicago, Illinois, heat wave that caused more than 700 deaths (Dematte et al. 1998).

Urban effects in mesoscale models can be represented using different techniques and parameterizations. The main goal is to take into account the impact of a city on momentum–turbulence processes and heat exchange. The first approach to modify the dynamics in the numerical models was increasing the roughness over urban areas assuming that turbulent fluxes are constant with height. In this technique, the vertical structure of the turbulent field is not reproduced in the urban roughness sublayer (from street level up to 50–100 m) and the effects of the city are limited to the surface level. The 2D hydrostatic, Boussinesq, vorticity-mode boundary layer model (Urban Meteorology PBL Model, URBMET) of Bornstein (1972, 1975) was the first to simulate flows over a warm and rough urban area. Simulations reproduced roughness deceleration at the upwind urban edge, UHI-induced maximum speeds at the downwind edge, and weakened the near-surface return flow downwind of the city.

The first attempt to account for the impact of urban environments on the surface energy budget was changing land-use properties. Best (1998) and Dupont et al. (2004) introduced more complex physical approaches where a sublayer representing the canopy is inserted between the surface and the atmosphere. The shadowing and radiation trapping effects of paved structures significantly modify the energy budget over cities. Reduction of the total albedo and nocturnal radiation loss caused by buildings is parameterized through the calculation of the energy budget for walls and streets where street direction and wind speed in the canopy are important factors. In standard versions of mesoscale models, some changes in soil thermal capacity are adopted over urban areas, but computation of surface energy balance does not take into account shadowing and radiation trapping effects.

The urban surface exchange parameterization developed by Martilli et al. (2002) incorporates the different techniques mentioned above to represent urban effects in mesoscale models. The parameterization accounts for impacts from horizontal and vertical building surfaces in the momentum, heat, and turbulent kinetic energy (TKE) equations. In these equations, new terms were included to represent frictional and drag forces' influence on the mean wind, changes on the potential temperature from sensible heat fluxes from urban surfaces, and the increase of the TKE from the airflow between buildings.

A comparison between measurements, outputs from the urbanized model, and results from a traditional scheme based on the constant flux-layer assumption of the Monin–Obukhov similarity theory was performed for momentum, TKE, and temperature fields to determine the accuracy of the new parameterization over Athens, Greece (Martilli et al. 2003). The urbanized approach was able to reproduce better the vertical structure of urban roughness sublayer parameters, distributing the sink of momentum from the surface up to the height of the highest building. The scheme properly simulated net radiation, canyon temperature, turbulent heat fluxes, and heat storage during the Basel Urban Boundary Layer Experiment (BUBBLE) and ESCOMPTE field campaign in Marseille, France (Hamdi and Schayes 2005). Vertical potential temperature profiles showed similar patterns of behavior to observations because of the scheme distributing heat sources in the vertical up to roof height. Atmospheric warming in the early morning was delayed as a result of heat storage of impervious surfaces. An evaluation with measurements from the Dual-Use European Security IR Experiment (DESIREX 2008) field campaign in Madrid, Spain, demonstrated the capability of the parameterization to accurately simulate the spatial and temporal distributions of the UHI and the contribution of anthropogenic heat to its magnitude and extension (Salamanca et al. 2012).

The aim of this work is to evaluate urban modeling with the Weather Research and Forecasting (WRF) Model for New York City, New York (NYC), during an intense heat-wave event in summer 2010 when using a multilayer urban parameterization customized for NYC coupled to an energy building model. Gridded urban canopy parameters (UCPs) were assimilated, and the land cover land-use (LCLU) was modified to improve the representation of the city's urban morphology. The performance of the temporal and spatial simulations of surface temperatures and wind fields of three urban parameterizations are tested and validated against observations.

The paper's organization presents first a description of the WRF modeling system and initialization process using UCPs followed by a comparison of the large-scale forcing from a regional model and weather maps. The analysis of the results was focused on 6 July, on which day the maximum temperatures were registered. We reference the generations of horizontal roll vortices and the impact of model resolution and time step on their characteristics. In the final section, we show and discuss modeled vertical profiles at the location of the highest buildings within the city.

2. Data and methodology

a. Modeling system

The WRF Model is a nonhydrostatic, compressible model with a mass coordinate system in which land surface models (LSMs) use surface boundary layer scheme variables, radiation scheme variables, and precipitation from microphysics and convective schemes, together with input parameters concerning land surface properties, to provide surface heat and moisture fluxes (Skamarock et al. 2008). The Noah LSM (Chen and Dudhia 2001) predicts soil temperature and moisture, diagnoses skin temperature and forest canopy moisture, and provides composite sensible and latent heat fluxes to the planetary boundary layer (PBL) scheme. Urban grid cells in this scheme are assumed to be flat, impervious open spaces with small albedos, large surface roughness, and 5% of vegetation. More complex schemes are available in WRF to represent the environmental effects of urban areas.

The Building Energy Parameterization (BEP), available since version 3.1 of WRF, accounts for impacts from ground surfaces, as well as from horizontal and vertical building surfaces, in the PBL prognostic momentum, heat, and TKE equations (Martilli 2002). This parameterization simulates building drag effects, transformation of mean-motion kinetic energy into TKE, and heat flux modification due to radiative shadowing and radiation effects. Urban grid cells are assumed to be composed of an array of buildings of the same width located at the same distance from each other, but with different heights. BEP does not account for any type of anthropogenic heat sources.

The Building Energy Model (BEM; Salamanca and Martilli 2010) calculates the amount of heat that has to be extracted from or added to each building floor to maintain the indoor temperature at a target value. BEM accounts for natural building ventilation, heat diffusion between indoor and outdoor surfaces, generation of heat due to occupants and equipment, and the energy consumption and associated production of waste heat from air conditioning (A/C) systems. A/Cs are considered to be through-wall equipment, and anthropogenic heat is released in each model layer.

b. Urban canopy parameters

The lookup table approach, which is traditionally used to initialize the multilayer urban schemes, underestimates the heterogeneity of the urban morphology by assigning average UCPs to each urban class. Detailed building information improves 2-m air temperature forecast and anthropogenic heat estimations (Salamanca et al. 2011). In this work, a technique that combines gridded data and lookup tables was implemented using UCPs from the National Urban Database and Access Portal Tool (NUDAPT) to obtain a better representation of the spatial distribution of building in NYC. NUDAPT consists of a set of 13 building statistics computed at a 250-m spatial resolution, including mean building height, height histograms, plan area fraction, height to width ratio, and sky factor (Burian et al. 2008). For the NYC area, these data are available only for Manhattan, and small sections of Queens, Brooklyn, and New Jersey adjacent to Manhattan.

Gridded NUDAPT data were assimilated for Manhattan, and they was also used to calculate mean UCPs corresponding to three urban classes (low residential, high residential, and commercial) to represent building characteristics in the rest of the domain. The main limitation of the table is that the UCPs are overestimated, reducing the proper simulation of the UHI effect in Manhattan. For those parameters that were not available on NUDAPT, such as heat capacities and thermal conductivities of roofs, walls, and ground, standard values employed by Roberts et al. (2006) during their urban heat storage study in Marseille were adopted.

LCLU is an important component in accurately simulating urban meteorological impacts. The LCLU classification available includes three urban classes from the 2001 U.S. Geological Survey National Land Cover Dataset (NLCD). Their criteria for categorizing a region as urban are the same for the whole United States, which leads to an underestimation of the spatial variations in highly heterogeneous cities. A new LCLU classification was thus incorporated based on the distribution of the Building Plan Area Fraction (Lambda P), which is defined as the plan area of buildings divided by the total surface area (Fig. 1). The modified classification was created by categorizing as low residential, high residential, and commercial those grid cells with Lambda P between 0.001 and 0.2, between 0.2 and 0.4, and greater than 0.4, respectively. A correction for Central Park was also implemented to substitute grid points within the park erroneously classified as urban. In the corrected

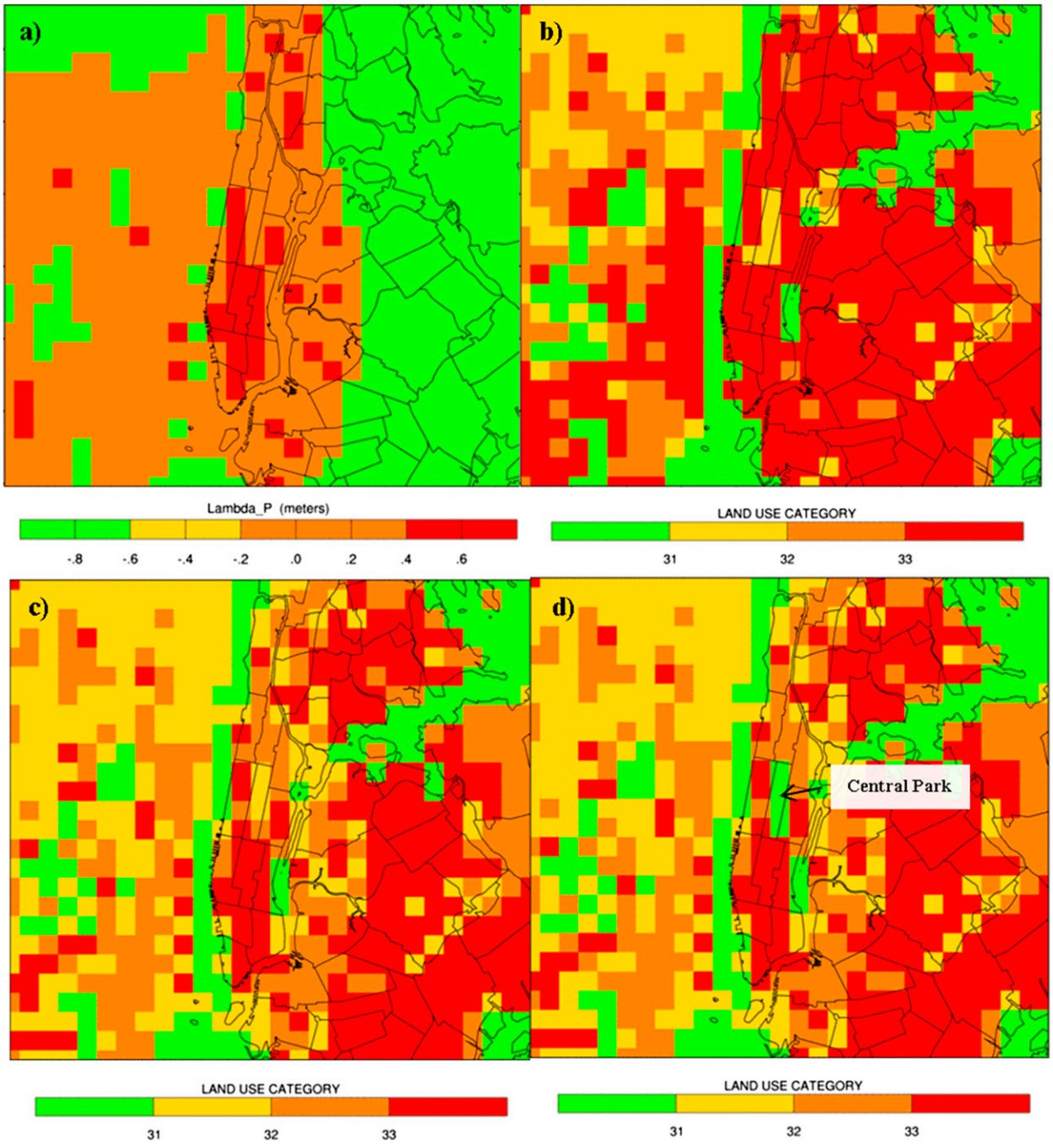

FIG. 1. (a) Building plan area fraction gridded (Lambda P) data distribution, (b) NLCD for NYC, (c) modified LC classification, and (d) correction for Central Park. Urban classes are land use category: low residential (31), high residential (32), and commercial (33).

classification, only highly dense urban areas inside Manhattan are classified as commercial while the rest of the domain is classified as low or high residential.

c. *Observational data*

Surface information from 36 weather stations (Fig. 2) provided by Earth Networks, Inc., was interpolated using the kriging method to obtain arrays that matched the spatial and temporal grids of the 1-km WRF domain output. Data from this network have been previously employed by Hicks et al. (2012, 2013) to analyze urban turbulence. Although representativeness of the surface station information deserves a detailed exploration on a station-by-station basis, for the purpose of this study and

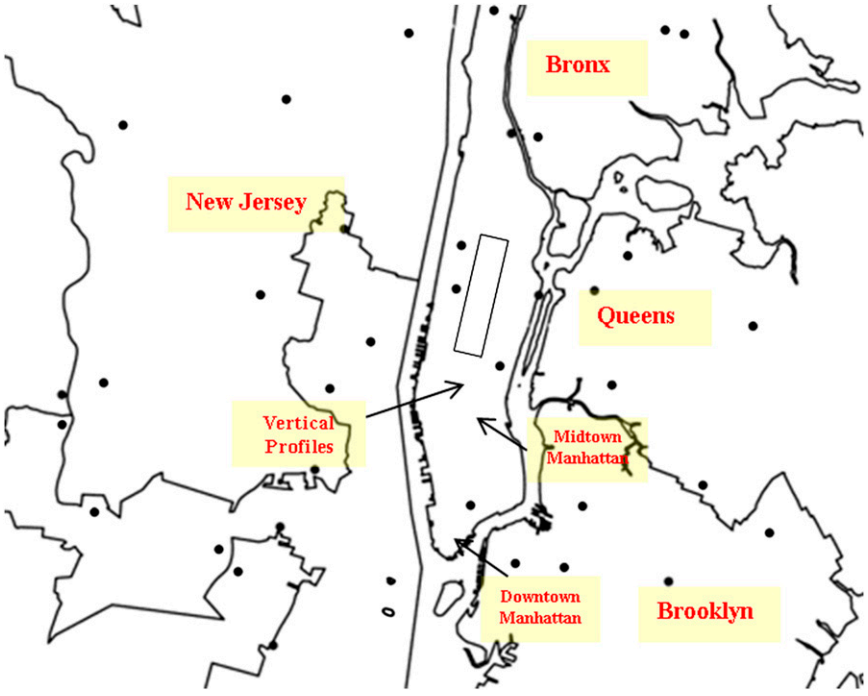

FIG. 2. Surface weather station network.

in the spirit of providing high spatial resolution observations, we will not concern ourselves with bias corrections.

d. Model configuration and numerical simulations

The Advanced Research configuration of WRF, version 3.2, was used to simulate the 3-day heat-wave event over NYC from 5 to 8 July 2010. Three two-way nested domains were constructed with spatial grid resolutions of 9, 3, and 1 km, which contained 150×150, 150×150, and 100×100 grid boxes, respectively, from west to east and from north to south (Fig. 3). Fifty-one terrain following sigma levels were defined with 20 levels in the first kilometer. The PBL scheme of Bougeault and Lacarrere (1989) was adopted. This turbulent kinetic energy prediction option was designed for use with BEP and BEM urban models. The single-moment three-class (Hong et al. 2004) and Kain–Fritsch (Kain and Fritsch 1990) schemes were the microphysics and cumulus options selected. The cumulus parameterization was only applied to the coarse domain and the first nest. For longwave and shortwave radiation, the RRTM (Mlawer et al. 1997) and Dudhia (Dudhia 1989) schemes were used. The initial and boundary conditions for WRF were obtained from the North American Mesoscale Model (NAM) datasets with 12-km resolution at 3-h intervals. NCEP Marine Modeling and Analysis Branch data at 0.5° were employed to update the sea surface temperatures every 24 h.

Four simulations with different configurations were performed. In the first simulation (No City), the city was replaced by grassland in the third domain to estimate the magnitude of the heat wave. In the second run (BEP), WRF coupled with BEP was used to analyze the interaction between the urban heat island effect caused by the properties of the city and the heat wave. A third simulation including BEM was performed to determine the impacts of energy consumption. This simulation is referred as BEP/BEM. Last, the importance of the

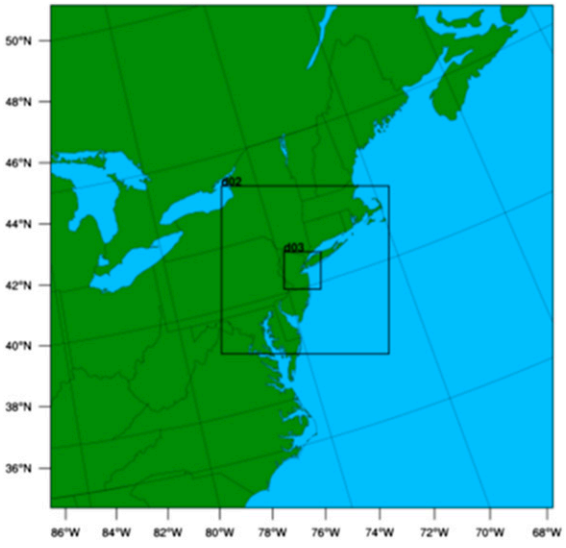

FIG. 3. Model domains. The larger rectangle is domain d02 and the smaller one is d03.

complexity of the urban parameterization was analyzed by only using the Noah land surface model.

e. Large-scale forcing

Similar to the synoptic pattern described by Kunkel et al. (1996) for the 1995 Chicago heat wave, the weather conditions during the Northeast event were dictated by a strong subtropical ridge that developed over the East Coast starting on 5 July (Fig. 4). At 500 hPa, the ridge covered most of the East Coast, showing intensification on 6 July with the presence of an upper-level closed anticyclone. The ridge and the associated closed high weakened and moved westward during the following day, producing a shift in the wind direction to the northeast that advected cool air to the area.

At the surface, strong and persistent anticyclonic conditions predominated in the development of the heat wave (Fig. 5). The strong subsidence produced surface high temperatures that reached values of 311 K in Manhattan and magnitudes over 305 K in Queens, Brooklyn, and the Bronx. The peak of the heat event was characterized by an intense high pressure system over the East Coast and part of the ocean that induced a weak westerly wind that advected warm air into the area. Following the trajectory of the upper-level subtropical ridge, the surface high showed westward movement dissipating by the end of 8 July. A surface low coupled with a trough at 500 hPa formed on 7 July and moved into the eastern United States, intensifying the following day. The presence of the low pressure system produced a shift in the wind direction from northwest to east-northeast on the early morning of 8 July, bringing cool air from the ocean to the East Coast and decreasing the surface temperatures. The heat-wave synoptic pattern was no longer present in the area that marked the conclusion of the heat event.

NAM was able to represent the key predictors associated with the heat wave but showed some differences with respect to what is seen on the weather maps. The intensity of the subtropical ridge in the upper air for the entire period was slightly overestimated by the NAM model (Fig. 4). However, this difference does not drastically affect the wind speed or direction. The location and the westward motion of the upper-level high retained a close resemblance to the behavior presented in the synoptic maps. At this level, temperatures are about one degree colder than observations for the first day of the event while for the rest of the period the values remained close to the registered upper-air temperatures. At the surface, the modeled circulation is similar to the wind patterns present on 5 and 6 July (Fig. 5). By the next day (7 July), a low pressure system moving from the east, changed the wind pattern, and introduced cooler marine air to the area. The shift in the wind direction to a northeast component in the model occurred 12 h before decreasing temperatures over the region. The regional model captured the higher temperatures over highly urbanized areas like NYC, Philadelphia, Pennsylvania, and the New Jersey coast.

3. Urban parameterization evaluation

a. Surface air temperature

The National Weather Service (NWS) declares heat watches and warnings in a region when the daytime heat index, an expression that combines temperature and relative humidity, is greater than or equal to 105°F (40.6°C), with nighttime lows greater than or equal to 80°F (26.7°C), for at least two consecutive days (NWS 1994). Mean observed and modeled hourly surface temperature values for the heat wave in NYC were calculated. The heat index time series obtained from observations (Fig. 6) showed maximum values of 42°, 48°, and 44°C and minimum values of 30°, 30.5°, and 28°C for three consecutive days in clear correspondence with the NWS's heat-wave definition.

The impact of urbanization is analyzed through the replacement of pavement by vegetation and the different techniques used to account for urban canopy interactions. Figure 6 also shows the time series of the hourly averaged 2-m air temperature for all of the stations and the nearest-neighbor grid points in each simulation. In general, BEP/BEM was more accurate in predicting the temperatures in the area at the peak of the heat-wave event with and overestimation on the first day. The similarity of the Noah and No City cases throughout the simulation revealed a minimal effect of the land surface urbanization properties within Noah for this event. BEP's accelerated nighttime rate of cooling produced minimal temperatures that reached magnitudes colder than the case with only vegetation and a difference of 2°–3°C relative to observations.

Gedzelman et al. (2003) found that around NYC, the urban–rural temperature difference is greatest on clear nights with low humidity and gentle northwest winds, but it is strongly reduced by sea breezes and cold air advection during summer. The advection of cool marine air—induced on the large-scale forcing by the early change of wind to a northeast direction as referenced above—introduced colder air to the city that lowered the temperature by as much as 3°–4°C over the region throughout 7 July. The heat released by A/C systems was not enough to compensate for the intense cooling produced by the cold advection.

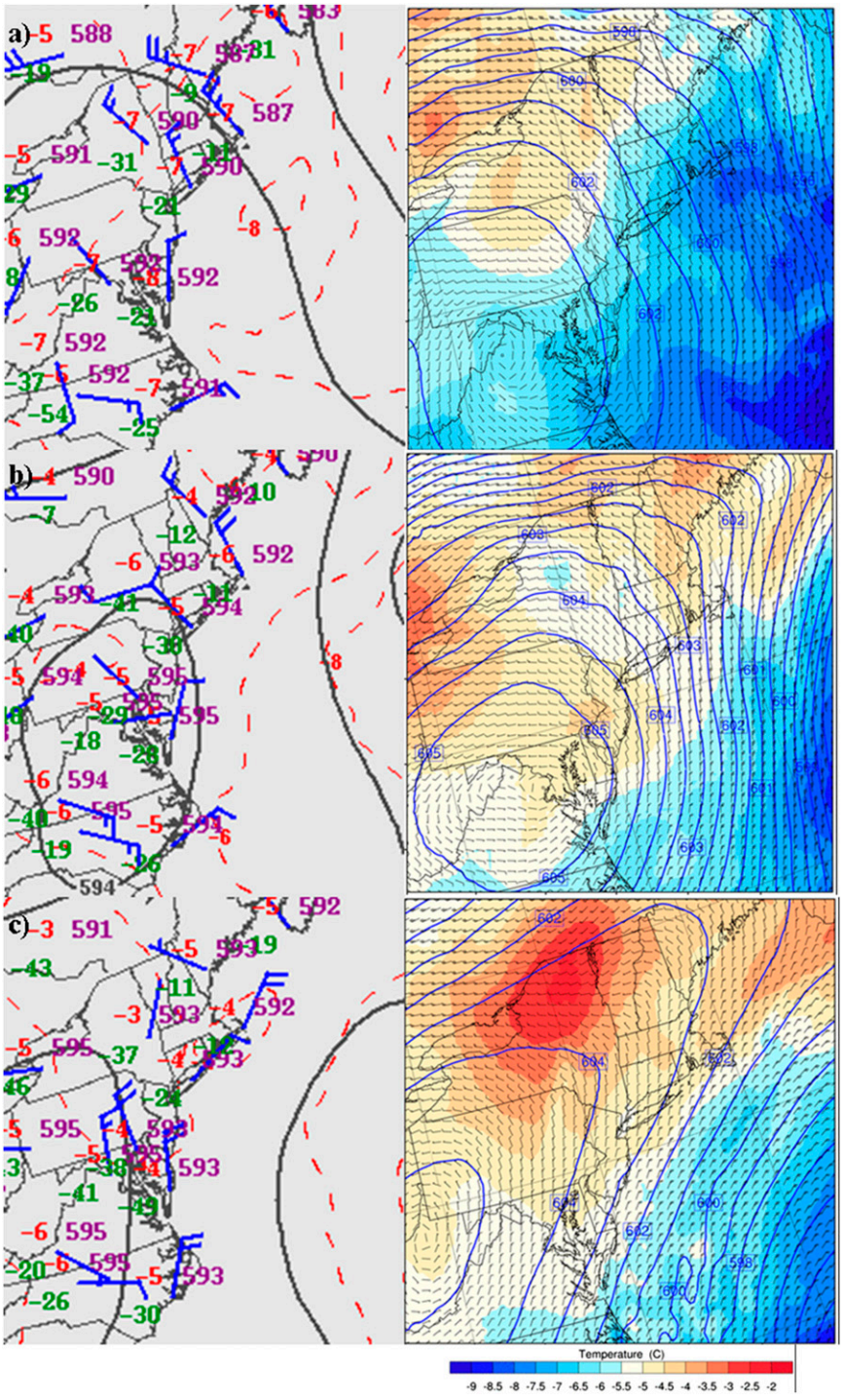

FIG. 4. The (left) 500-hPa maps and (right) corresponding NAM outputs at 1200 UTC on (a) 5, (b) 6, and (c) 7 Jul.

b. Surface temperature and wind spatial distribution

Differences in the temperature field between observations and model simulations are examined at 0600 and 1500 LT 6 July. At the time of the minimum temperature (Fig. 7), the No City and Noah LSM cases showed an almost similar temperature distribution between each other with Noah introducing some warming at downtown Manhattan and Brooklyn. BEP/BEM constitutes the parameterization that better represents the spatial

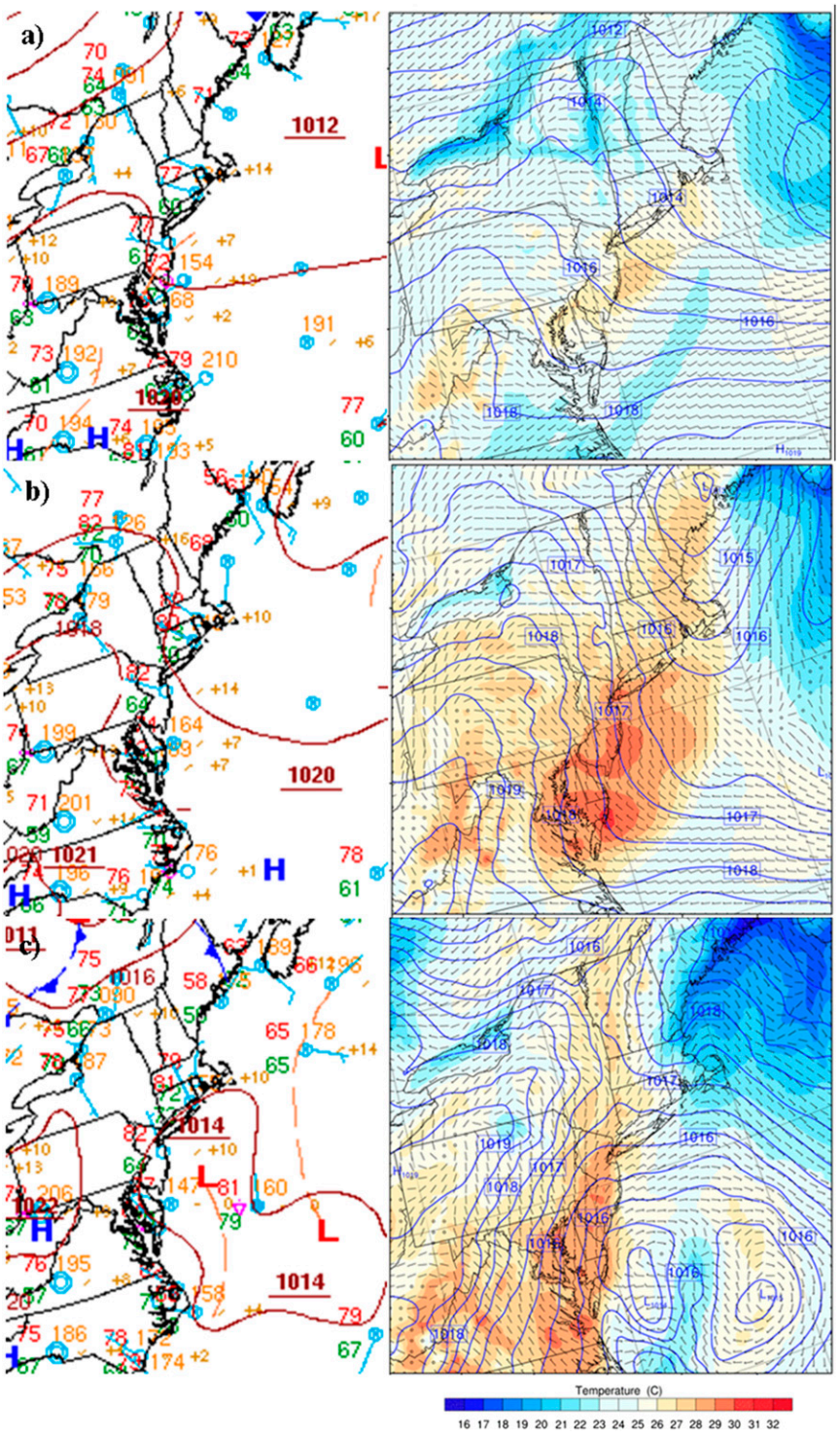

FIG. 5. As in Fig. 4, but for surface maps.

distribution of the temperature for the region where detailed building information was available. All other models underestimate the temperature over NYC, following the tendency that was also found by Holt and Pullen (2007) for August 2005 using a single (Kusaka et al. 2001) and a multilayer (Brown and Williams 1998) urban scheme in COAMPS. The anthropogenic heat released by BEP/BEM counteracted the nighttime excessive

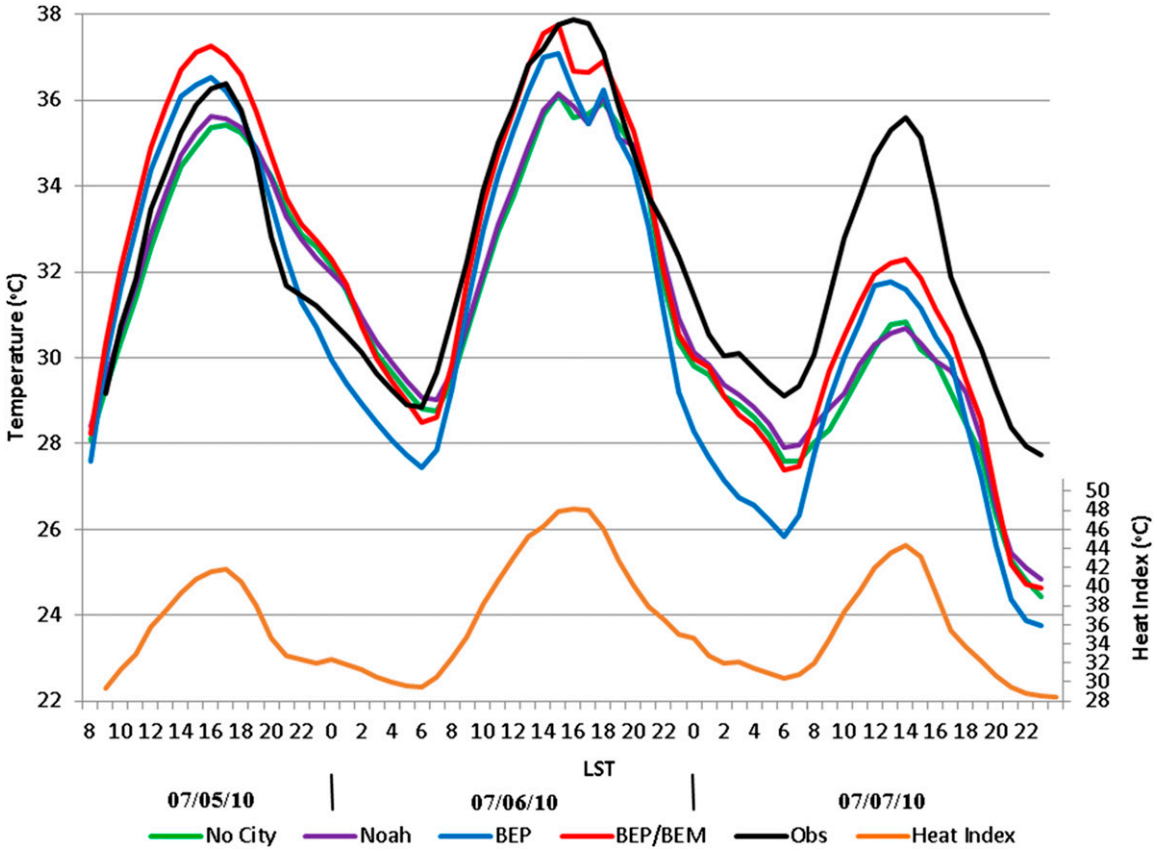

FIG. 6. Observed and modeled (top) surface temperature and (bottom) heat index time series from 5 to 7 Jul.

cooling. In some regions of the city, the heating increased the ambient temperature to magnitudes that surpassed measured values. BEP cold bias is evenly distributed across the domain with cooler magnitudes matching the location of the tallest building areas in Manhattan.

Nighttime negative heat flux is enhanced by the introduction of city morphology with the greatest values at the location of the tallest buildings (Fig. 8). BEP's building internal temperature is fixed at 25°C throughout the whole simulation, producing a heat flux from the warmer outside to the cooler inside decreasing the outdoor temperature. BEP/BEM uses an A/C system to cool down the building's interior, releasing heat into the atmosphere. This heat addition compensated the negative flux, increasing the outdoor temperature to a magnitude closer to the observations. The amount of heat released is proportional to the building heights with maximum values that doubled the modeled estimations obtained by Sailor and Hart (2006) for NYC. According to their empirical model based on electricity, heating fuel, transportation, and metabolism data, summertime hourly average anthropogenic heat is about 69.4 $W m^{-2}$, while our simulations indicate average values around 100 $W m^{-2}$.

In addition to those areas of Brooklyn, Queens, and the Bronx where overestimation was expected because of a lack of proper urban canopy parameters, BEP/BEM results over commercial zones with high buildings in Manhattan are warmer than observations by more than 2°C in the afternoon (Fig. 9). Salamanca et al. (2011) using BEP/BEM obtained for the city of Houston an increase in air temperature of 0.5°–2°C, which they attributed to the waste heat produced by the energy consumption inside the buildings.

Mean and turbulent wind velocity fields are modified by the buildings' barrier effect, as well as rougher urban surfaces that increase the frictional drag on the flow (Bornstein 1987). Figure 10 shows the surface winds at the time of minimum temperature and the difference from the interpolated observations. A northwesterly component was dominant at this time of the day with a divergence zone west of Manhattan in the No City case, which is attenuated in the urban cases. When urbanization was introduced, the wind direction was not altered regardless of the roughness increase or building presence, as all simulations maintain the same orientation of the flow. However, a prominent decrease in the wind speed was observed. In this region, the wind speed

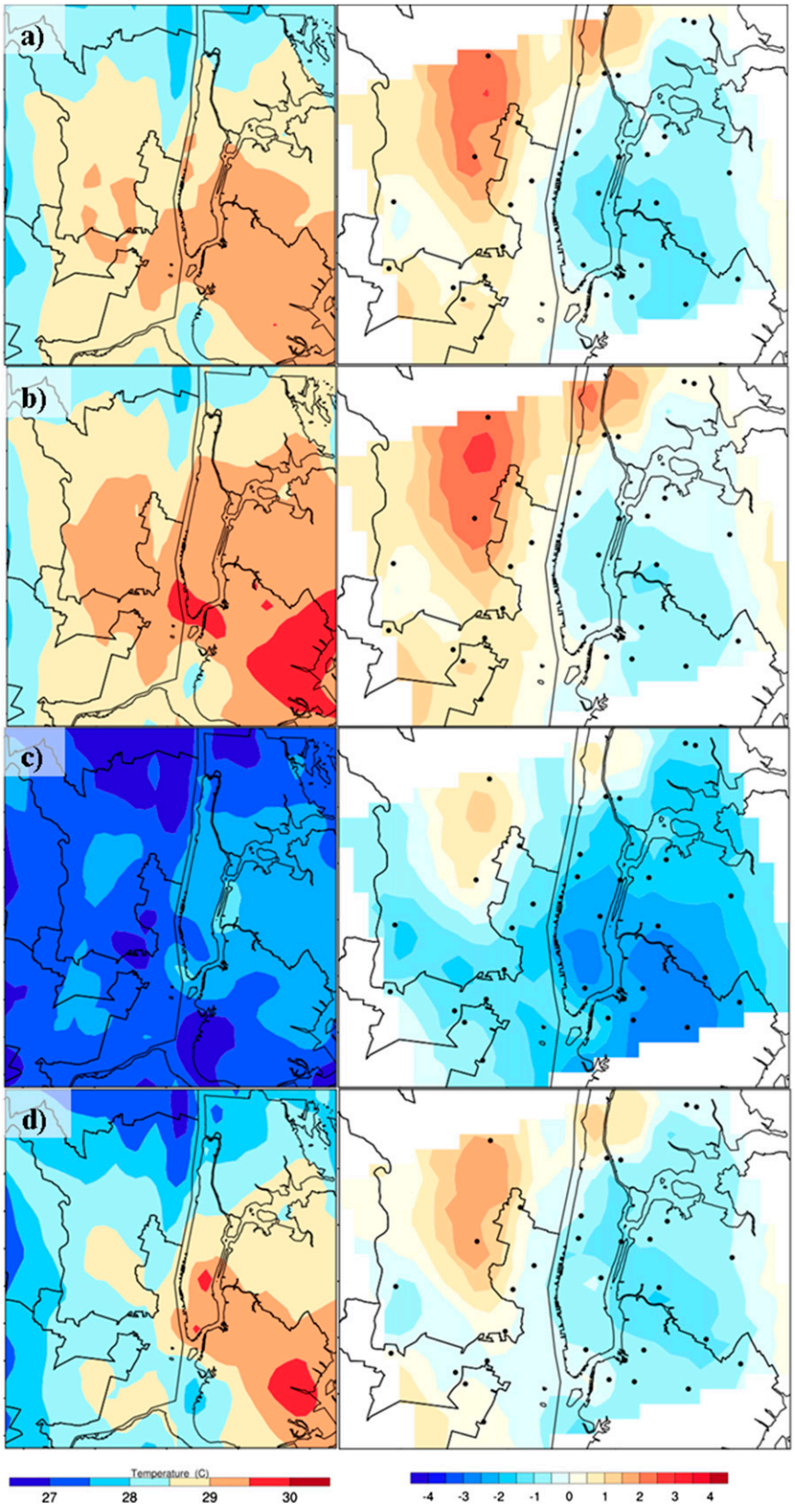

FIG. 7. (left) Temperature distribution and (right) temperature difference between observations and model output at 0600 LST 6 Jul for (a) No City, (b) Noah, (c) BEP, and (d) BEP/BEM.

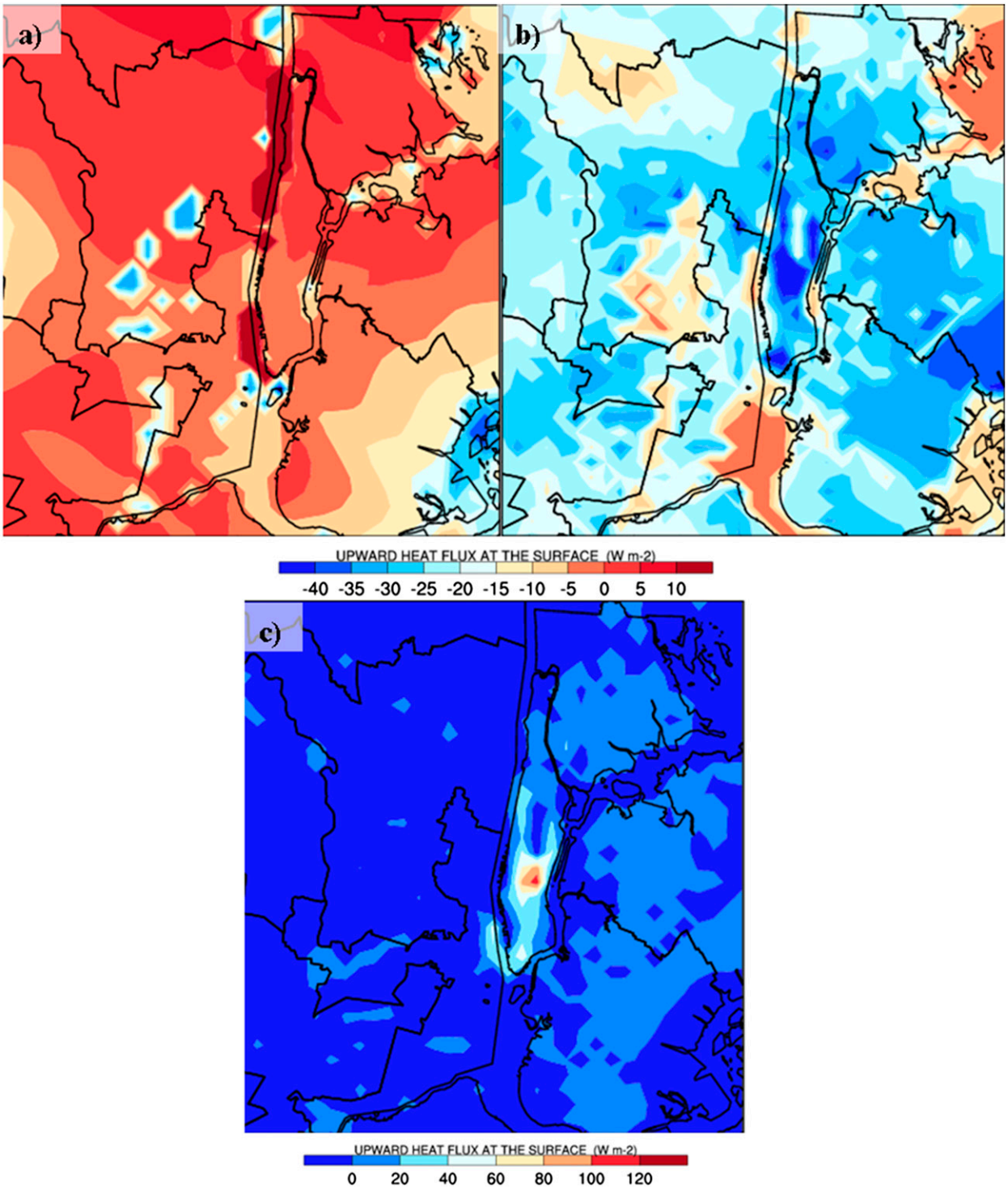

FIG. 8. Sensible heat flux at 0600 LST for (a) Noah, (b) BEP, and (c) BEP/BEM.

has strongly declined over the century as a result of the increase in building heights intensifying the UHI (Gaffin et al. 2008). The blocking effect of the buildings in the BEP and BEP/BEM cases reduced the magnitude of the wind flow by 1–2 m s^{-1} relative to observations over Manhattan. The extra heat generated by the A/C systems originated as a thermal gradient that accelerated the flow from New Jersey into the city, improving the

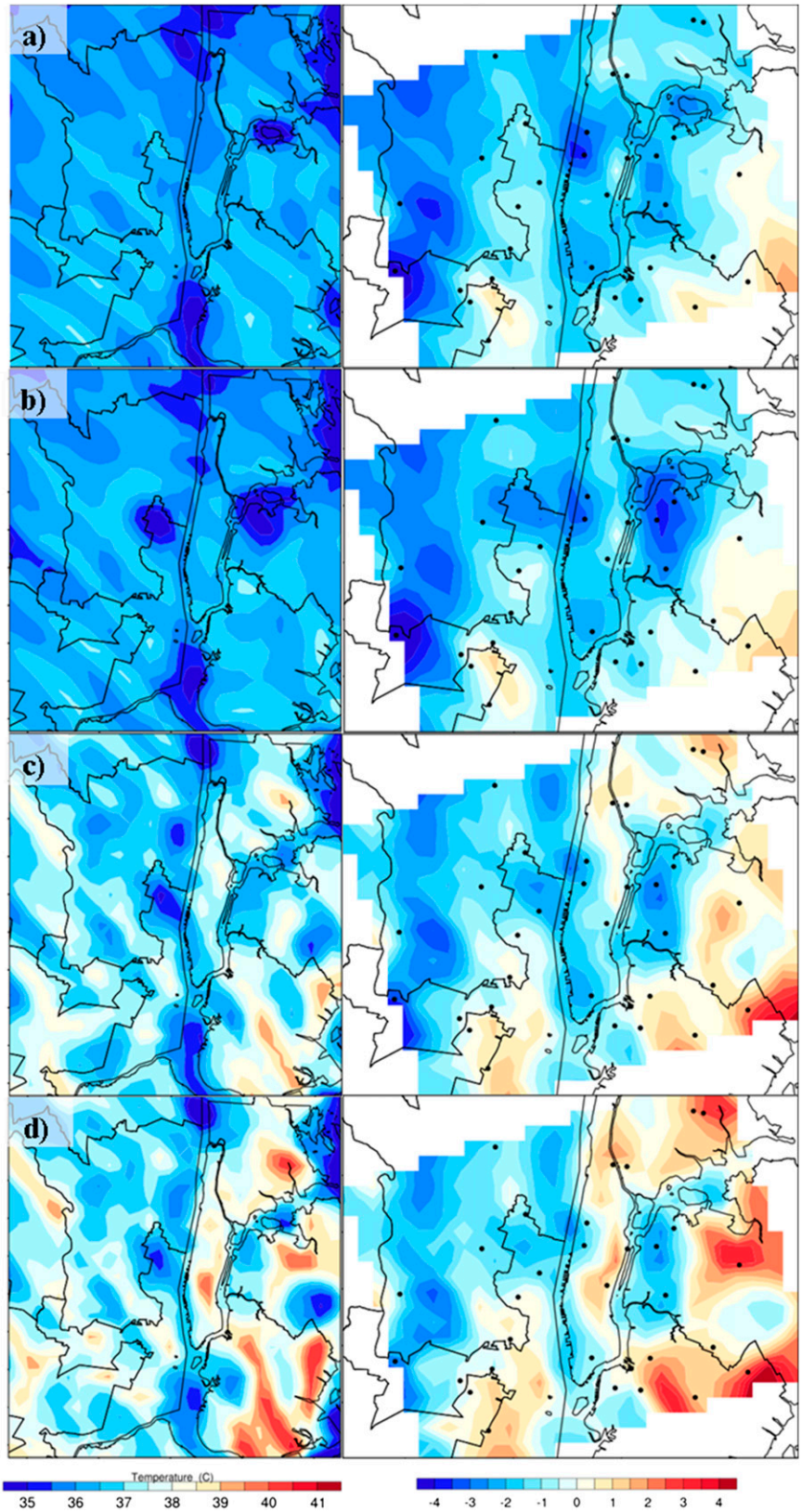

FIG. 9. (left) Surface temperature distribution and (right) temperature difference between observations and model output at 1500 LST 6 Jul for (a) No City, (b) Noah, (c) BEP, and (d) BEP/BEM.

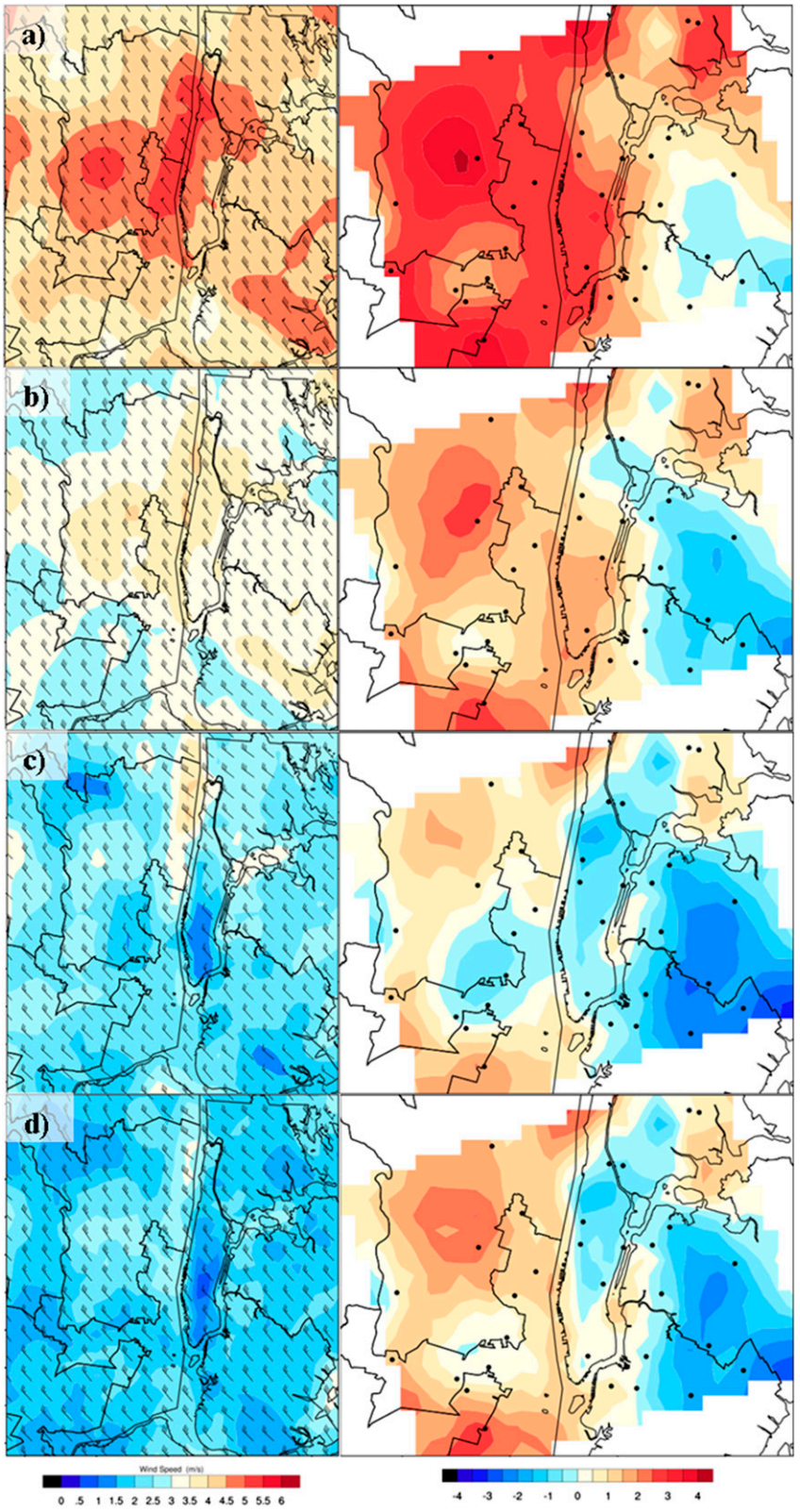

FIG. 10. As in Fig. 9, but for surface wind speed.

representation of this field in the BEP/BEP simulation. In the afternoon (Fig. 11), the northwesterly flow intensified, reaching values above 5 m s^{-1}, but slowing down when it entered Manhattan as a result of the building effect. The wind speed decrease was more pronounced where the highest buildings are located. The largest sources of error were centered on divergence zones in the model results that are absent in the interpolated data. BEP and BEP/BEM cases, which share identical building distributions, presented similar wind patterns. Under calm synoptic flows, the UHI produces inward-directed country breezes that result in speed maxima and confluence over the city (Bornstein and Johnson 1977). The excess of heat in the city and the associated thermal gradient did not accelerate the flow toward the city at this time of the day. The underestimation of the thermal gradient could be related to the misrepresentation of the UCPs in the areas surrounding NYC that prevented the formation of a breeze from the suburban areas.

The temperature and wind fields showed the formation of horizontal roll vortices (HRVs) in the afternoon (Fig. 12). At the time of maximum convection, these features enhance the vertical transport of momentum, heat, and moisture in the PBL. A series of sensitivity tests were performed for the NYC heat-wave case to determine some of the characteristics of these structures. A decrease in grid spacing intensified and multiplied rolls over the region. A time step reduction weakened the vortex strength and increased its size, leading to their dissipation when 1/54 of the recommended time step value was used. In a simulation for the entire month of July (figure not shown), HRVs were present every day at the time of the maximum temperature.

The HRVs' dependence on resolution and time step and their frequency could indicate that they may be related to numerical errors in the model. Changes in roll size and intensity due to variations in the resolution and time step are a consequence of modeling flows at resolutions that are too high to justify the PBL schemes used and yet are too coarse for an explicit calculation of turbulent transfer (Ching et al. 2014). However, these structures appear to have been observed through direct measurements and satellite images. Miao and Chen (2008) and Miao et al. (2009) reported cloud streets in visible satellite imagery related to HRV formation in Beijing, China, generated by WRF simulations. LeMone at al. (2010) claims to have found an appropriate correspondence between these convective boundary layer structures and the cloud streets in satellite images in terms of orientation, spacing, and timing for the IHOP 2002 field campaign in southeast Kansas. This topic needs further investigation to determine the reliability of the formation of vortices in WRF simulations. Our goal was to show that HRVs were present during unstable condition throughout the simulation period and we considered that it to be beyond the scope of this paper to explore this topic in detail.

c. *Vertical profiles at highest building location*

The vertical distribution of temperature over NYC is characterized by an absence of a surface inversion or relatively weak elevated inversion layers over the city and an excess in urban temperature that decreases rapidly with height (Bornstein 1968). Figure 13a shows modeled vertical potential temperature profiles at night (0300 LST) and during the day (1500 LST) at the locations of the highest buildings in midtown Manhattan. Unstable conditions dominated during nighttime in the lower troposphere according to BEP/BEM, which located the temperature inversion at a height of 400 m. The enhanced cooling generated by BEP produced a stable boundary layer while the conditions remained neutral in the No City case at the first 250 m. A slightly deeper neutral layer was also present in the Noah case, with an inversion at 350-m height. The anthropogenic heat released by BEP/BEM substantially increased the surface temperature, as shown by the spatial plots. The injected heat deepened the lapse rate in the first 100 m during daytime and nighttime.

The drag force distribution along the vertical generated a wind profile on the urban canopy that followed the urban model simulations of Roulet et al. (2005), who found a deceleration of the flow field resulting from the presence of obstacles and the log-type profile in nonurban areas obtained by Rotach (1993) from field measurements. At the building level, the wind speed was strongly influenced by city morphology on BEP and BEP/BEM (Fig. 13b). The urban surface roughness length in Noah reduced the magnitude of the wind by 1.5 m s^{-1} compared to the case with an absence of an urban environment. Above the urban canopy layer during nighttime, the wind vertical profiles were similar between the different cases. However, multilayer cases during daytime produced a sheared environment with a maximum wind speed of 7.5 m s^{-1} at 300 m while the calculation by Noah and No City of the momentum sink only at the ground produced a log-type profile with a horizontal flow speed that was almost constant with height just above the surface.

In the multilayer parameterization, the maximum TKE was located near the average building height (Fig. 13c) where, as observed by Louka et al. (2000), the shear production term reaches its maximum, implying the greatest production of turbulence at that level. Surface drag only increased turbulence near the ground in the other two cases. During nighttime, the interaction of

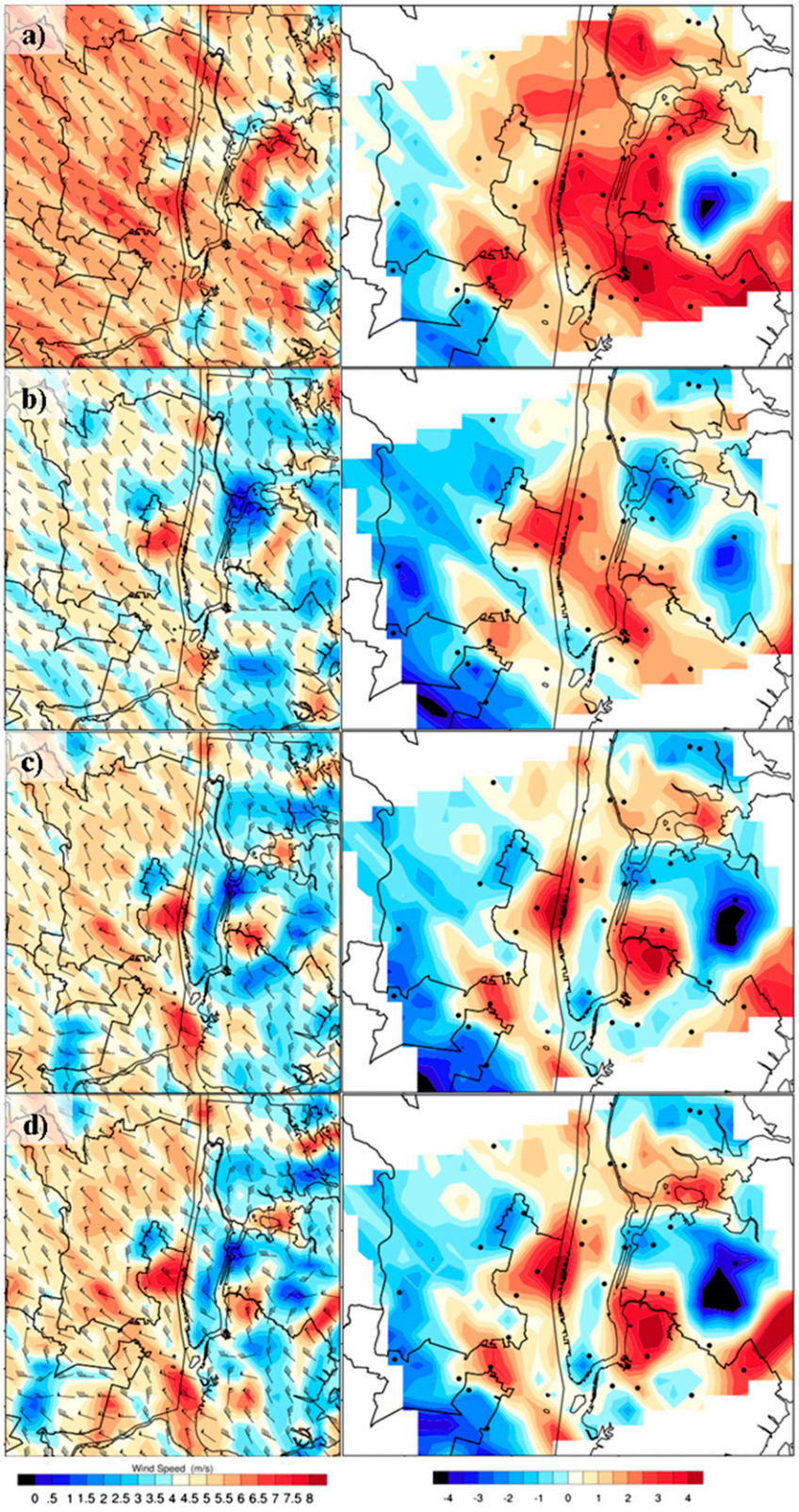

FIG. 11. As in Fig. 10, but for 0600 LST.

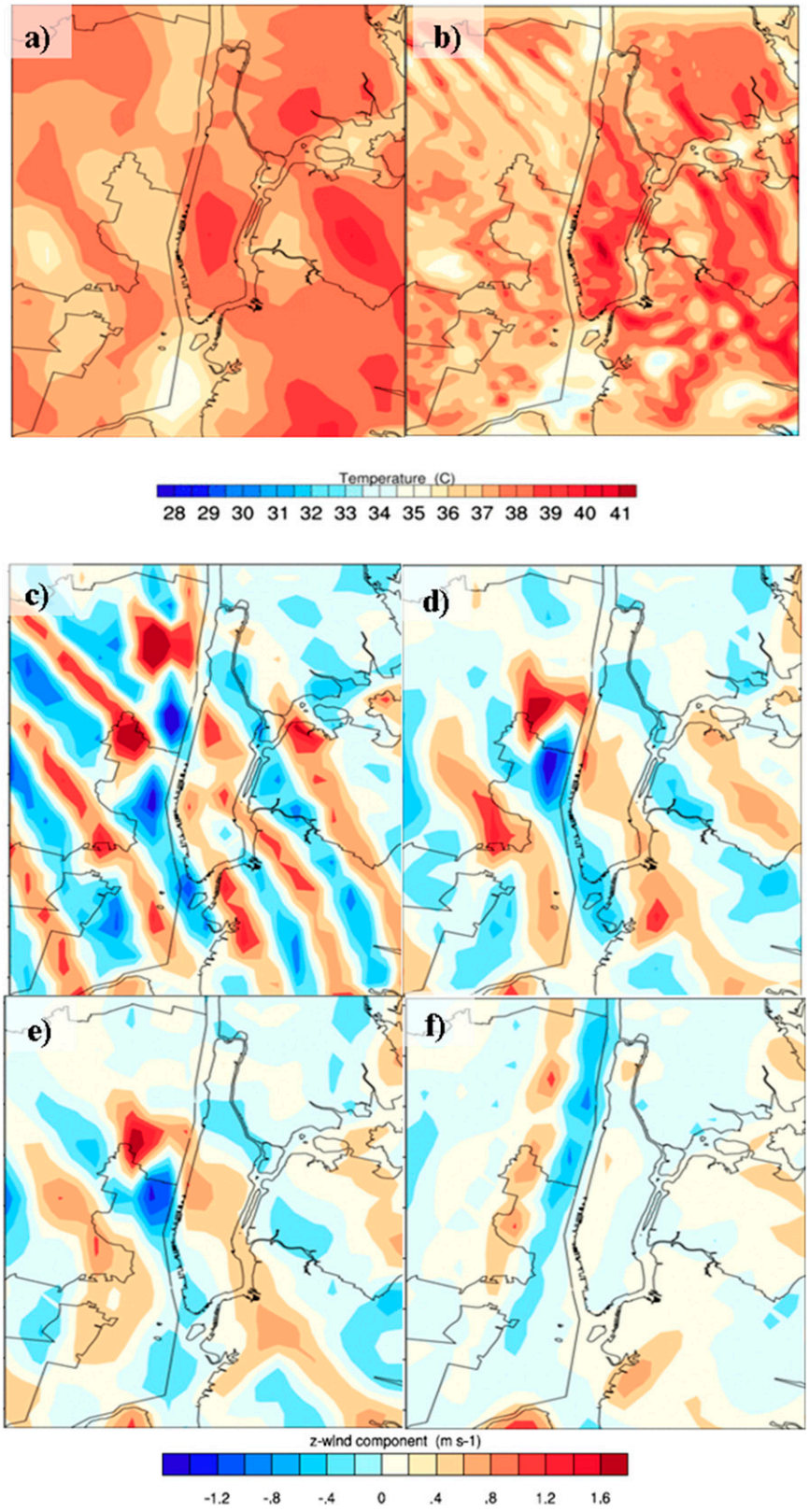

FIG. 12. Surface temperature at 1300 LST 6 Jul at altitudes of (a) 1 km and (b) 333 m. Vertical velocity at Δt = (c) 6, (d) 1, (e) 0.66, and (f) 0.11 s.

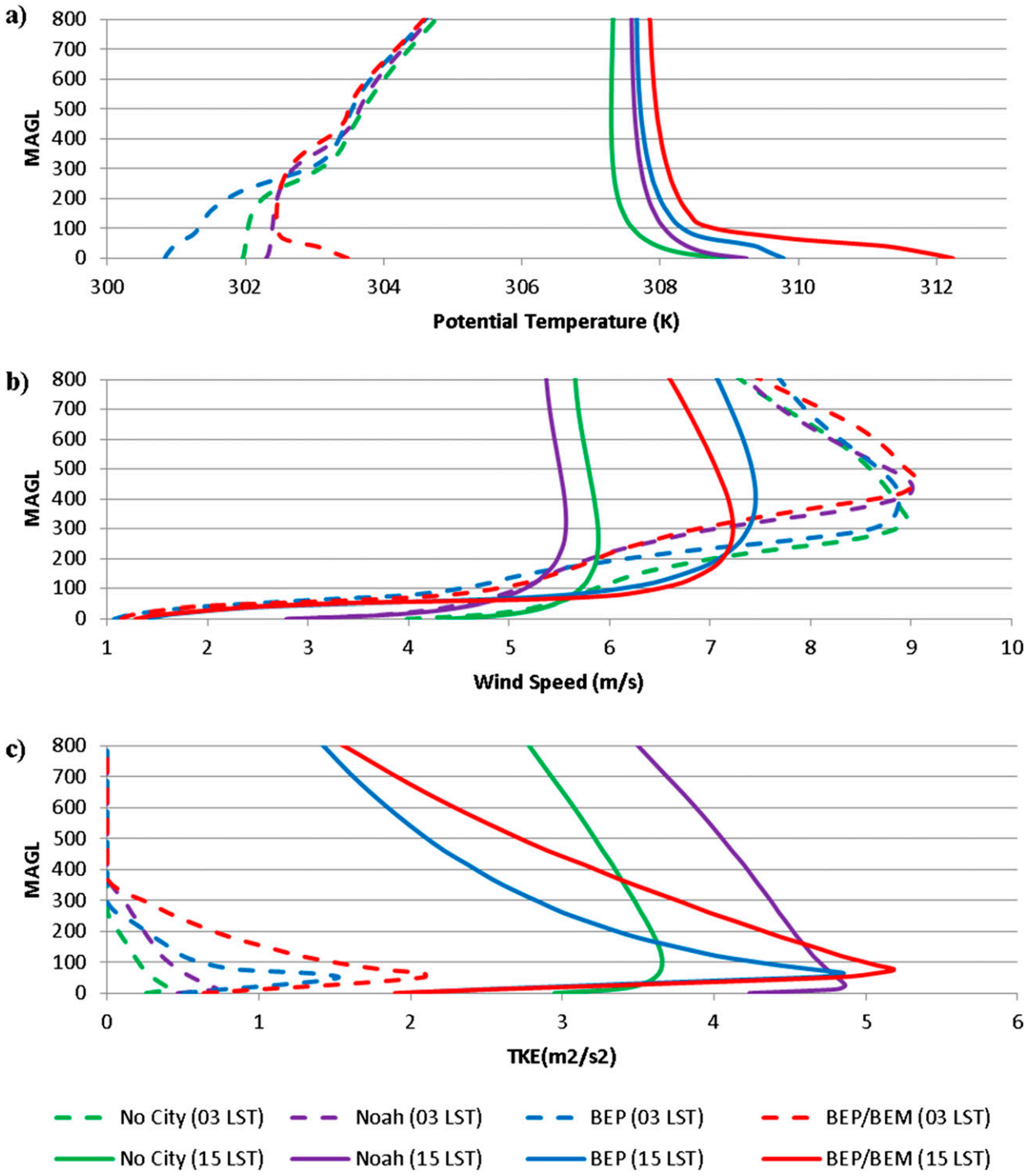

FIG. 13. Nighttime (dashes) and daytime (solid) vertical profiles at midtown Manhattan for (a) temperature (°C), (b) wind speed ($m\,s^{-1}$), and (c) TKE ($m^2\,s^{-2}$).

thermal and mechanical factors causes an increase in TKE in urban regions (Martilli 2002). The presence of the buildings mechanically induced the generation of TKE combined with the entrapment of radiation, which increased the vertical mixing. Anthropogenic heat enhanced TKE thermal production at the urban canopy layer, doubling its magnitude. A strong mechanically induced TKE close to ground level was shown during

daytime for the Noah and No City cases. On the other hand, turbulence in the multilayer schemes was inhibited below rooftop level. Turbulence is to a certain extent blocked inside the city canyon as a result of shear sheltering in the flow acceleration region above the roof level (Kastner-Klein et al. 2001). Thermal factors played a more important role above the building tops where heating from A/C systems contributed to turbulence magnifying TKE values.

4. Conclusions

Three urban parameterizations were examined over NYC during the days of a heat-wave event in summer 2010. The multilayer parameterization BEP coupled with the A/C system scheme BEM showed a more accurate representation of the temperature and wind fields in the urban canopy. Detailed high-resolution building information constitutes an important factor to correctly simulate meteorological parameters close to the surface over NYC under extreme summer heat conditions. In those areas where the lookup table was used, surface temperature was overestimated by several degrees Celsius as the wind speed was underestimated due to an enhancement of the building blocking effect. BEP's accelerated nighttime rate of cooling produced a decrease in nighttime temperature even more abrupt than the case where the city was replaced by vegetation. The heat exchange from the outside air toward the building walls and roofs was compensated by the heat waste generated from the BEM simulation's improving temperature estimation before sunrise.

The anthropogenic heat from AC systems strengthened the TKE, mainly above rooftops, where maximum turbulence was reached. Inversion height varied depending on the parameterization used. Temperature vertical profiles in the most complex urban scheme at the location of the highest building were characterized by steep lapse rates and the absence of an elevated inversion during nighttime. Horizontal roll vortices were present in the afternoon hours throughout the event. Sensitivity tests show a direct dependence on horizontal grid resolution and time step value. An increase in resolution enhanced the vortex strength whereas a time step reduction weakened these convective structures to the point of dissipation.

Acknowledgments. This research was supported, in part, by a grant of computer time from the City University of New York High Performance Computing Center under National Science Foundation (NSF) Grants CNS-0855217, CNS-0958379, and ACI-1126113. Partial financial support was provided by NSF Grant IIP-1439606. NCEP–NCAR reanalysis data were provided by the NOAA/OAR/ESRL PSD, Boulder, Colorado, from their website (http://www.esrl.noaa.gov/psd/).

REFERENCES

Anderson, B., and M. Bell, 2011: Heat waves in the United States: Mortality risk during heat waves and effect modification by heat wave characteristics in 43 U.S. communities. *Epidemiol. Rev.,* **119,** 210–218, doi:10.1289/ehp.1002313.

Best, M., 1998: Representing urban areas in numerical weather prediction models. Preprints, *Second Symp. on the Urban Environment,* Alburqueque, NM, Amer. Meteor. Soc., 148–151.

Bornstein, R. D., 1968: Observations of the urban heat island effect in New York City. *J. Appl. Meteor.,* **7,** 575–582, doi:10.1175/1520-0450(1968)007<0575:OOTUHI>2.0.CO;2.

——, 1972: Two dimensional non-steady numerical simulations of nighttime flow of a stable planetary boundary layer over a rough warm city. Preprints, *Conf. on Urban Environment,* Philadelphia, PA, Amer. Meteor. Soc., 89–94.

——, 1975: The two-dimensional URBMET urban boundary layer model. *J. Appl. Meteor.,* **14,** 1459–1477, doi:10.1175/1520-0450(1975)014<1459:TTDUUB>2.0.CO;2.

——, 1987: Mean diurnal circulation and thermodynamic evolution of urban boundary layers. *Modeling the Urban Boundary Layer,* Amer. Meteor. Soc., 53–93. [Available online at http://www.met.sjsu.edu/faculty/bornstein/old/urbanization/thermodynamic-URBANIZATION-1987.pdf.]

——, and D. S. Johnson, 1977: Urban-rural wind velocity differences. *Atmos. Environ.,* **11,** 597–604, doi:10.1016/0004-6981(77)90112-3.

Bougeault, P., and P. Lacarrere, 1989: Parameterization of orography-induced turbulence in a mesobeta-scale model. *Mon. Wea. Rev.,* **117,** 1872–1890, doi:10.1175/1520-0493(1989)117<1872:POOITI>2.0.CO;2.

Brown, M. J., and M. Williams, 1998: An urban canopy parameterization for mesoscale meteorological models. Preprints, *Second Symp. on the Urban Environment,* Albuquerque, NM, Amer. Meteor. Soc., 144–147.

Burian, S., N. Augustus, I. Jeyachandran, and M. Brown, 2008: Final report for the National Building Statistics Database, version 2. LA-UR-08-1921 Los Alamos National Laboratory, 78 pp. [Available online at http://glasslab.engr.ccny.cuny.edu/u/brianvh/UHI/NBSD2_FinalReport.pdf.]

Chen, F., and J. Dudhia, 2001: Coupling an advanced land surface–hydrology model with the Penn State–NCAR MM5 modeling system. Part I: Model implementation and sensitivity. *Mon. Wea. Rev.,* **129,** 569–585, doi:10.1175/1520-0493(2001)129<0569:CAALSH>2.0.CO;2.

Ching, J., R. Rotunno, K. LeMone, B. Kosovic, P. A. Jimenez, and J. Dudhia, 2014: Convectively induced secondary circulations in fine-grid mesoscale numerical weather prediction models. *Mon. Wea. Rev.,* **142,** 3284–3302, doi:10.1175/MWR-D-13-00318.1.

Dematte, J. E., K. O'Mara, J. Buescher, C. G. Whitney, S. Forsythe, T. McNamee, R. B. Adiga, and M. Ndukwu, 1998: Near-fatal heat stroke during the 1995 heat wave in Chicago. *Ann. Intern. Med.,* **129,** 173–181, doi:10.7326/0003-4819-129-3-199808010-00001.

Dudhia, J., 1989: Numerical study of convection observed during the Winter Mooson Experiment using a mesoscale two-dimensional model. *J. Atmos. Sci.,* **46,** 3077–3107, doi:10.1175/1520-0469(1989)046<3077:NSOCOD>2.0.CO;2.

Dupont, S., T. Otte, and J. Ching, 2004: Simulation of meteorological fields within and above urban and rural canopies with

a mesoscale model (MM5). *Bound.-Layer Meteor.,* **113,** 111–158, doi:10.1023/B:BOUN.0000037327.19159.ac.

Gaffin, S. R., and Coauthors, 2008: Variations in New York City's urban heat island strength over time and space. *Theor. Appl. Climatol.,* **94,** 1–11, doi:10.1007/s00704-007-0368-3.

Gedzelman, S. D., S. Austin, R. Cermak, N. Stefano, S. Partridge, S. Quesenberry, and D. A. Robinson, 2003: Mesoscale aspects of the urban heat island around New York City. *Theor. Appl. Climatol.,* **75,** 29–42, doi:10.1007/s00704-002-0724-2.

Hamdi, R., and G. Schayes, 2005: Validation of the Martilli's urban boundary layer scheme with measurements from two mid-latitude European cities. *Atmos. Chem. Phys. Discuss.,* **5,** 4257–4289, doi:10.5194/acpd-5-4257-2005.

Hicks, B., W. Callahan, W. Pendergrass, R. Dobosy, and E. Novakovskaia, 2012: Urban turbulence in space and in time. *J. Appl. Meteor. Climatol.,* **51,** 205–218, doi:10.1175/JAMC-D-11-015.1.

——, E. Novakovskaia, R. Dobosy, W. Pendergrass, and W. Callahan, 2013: Temporal and spatial aspects of velocity variance in the urban surface roughness layer. *J. Appl. Meteor. Climatol.,* **52,** 668–681, doi:10.1175/JAMC-D-11-0266.1.

Holt, T., and J. Pullen, 2007: Urban canopy modeling of the New York City metropolitan area: A comparison and validation of single-layer and multilayer parameterization. *Mon. Wea. Rev.,* **135,** 1906–1930, doi:10.1175/MWR3372.1.

Hong, S., J. Dudhia, and S. Chen, 2004: A revised approach to ice microphysical processes for the bulk parameterization of clouds and precipitation. *Mon. Wea. Rev.,* **132,** 103–120, doi:10.1175/1520-0493(2004)132<0103:ARATIM>2.0.CO;2.

Kain, J., and J. Fritsch, 1990: A one-dimensional entraining/detraining plume model and its application in convective parameterization. *J. Atmos. Sci.,* **47,** 2784–2802, doi:10.1175/1520-0469(1990)047<2784:AODEPM>2.0.CO;2.

Kastner-Klein, P., E. Fedorovich, and M. W. Rotach, 2001: A wind tunnel study of organized and turbulent air motions in urban streets canyons. *J. Wind Eng. Ind. Aerodyn.,* **89,** 849–861, doi:10.1016/S0167-6105(01)00074-5.

Kunkel, K. E., S. A. Changnon, B. C. Reinke, and R. W. Arritt, 1996: The July 1995 heat wave in the Midwest: A climatic perspective and critical weather factors. *Bull. Amer. Meteor. Soc.,* **77,** 1507–1518, doi:10.1175/1520-0477(1996)077<1507:TJHWIT>2.0.CO;2.

Kusaka, H., Y. Kondo, Y. Kikegawa, and F. Kimura, 2001: A simple single-layer urban canopy model for atmospheric models: Comparison with multi-layer and slab models. *Bound.-Layer Meteor.,* **101,** 329–358, doi:10.1023/A:1019207923078.

LeMone, M. A., F. Chen, M. Tewari, J. Dudhia, B. Geerts, Q. Miao, R. Coulter, and R. Grossman, 2010: Simulating the IHOP_2002 fair weather CBL with the WRF–ARW–Noah modeling system. Part II: Structures from a few kilometers to 100 km across. *Mon. Wea. Rev.,* **138,** 745–764, doi:10.1175/2009MWR3004.1.

Louka, P., S. E. Belcher, and R. G. Harrison, 2000: Coupling between air flow in streets and the well-developed boundary layer aloft. *Atmos. Environ.,* **34,** 2613–2621, doi:10.1016/S1352-2310(99)00477-X.

Martilli, A., 2002: Numerical study of urban impact on boundary layer structure: Sensitivity to wind speed, urban morphology, and rural soil moisture. *J. Appl. Meteor.,* **41,** 1247–1266, doi:10.1175/1520-0450(2002)041<1247:NSOUIO>2.0.CO;2.

——, A. Clappier, and M. W. Rotach, 2002: An urban surface exchange parameterization for mesoscale models. *Bound.-Layer Meteor.,* **104,** 261–304, doi:10.1023/A:1016099921195.

——, Y. Rouleta, M. Juniera, F. Kirchnera, M. Rotachb, and A. Clappier, 2003: On the impact of urban surface exchange parameterisations on air quality simulations: The Athens case. *Atmos. Environ.,* **37,** 4217–4231, doi:10.1016/S1352-2310(03)00564-8.

Meehl, G., and C. Tebaldi, 2004: More intense, more frequent, and longer lasting heat waves in the 21st century. *Science,* **305,** 994–997, doi:10.1126/science.1098704.

Miao, S., and F. Chen, 2008: Formation of horizontal convective rolls in urban areas. *Atmos. Res.,* **89,** 298–304, doi:10.1016/j.atmosres.2008.02.013.

——, ——, M. LeMone, M. Tewari, Q. Li, and Y. Wang, 2009: An observational and modeling study of characteristics of urban heat island and boundary layer structures in Beijing. *J. Appl. Meteor. Climatol.,* **48,** 484–501, doi:10.1175/2008JAMC1909.1.

Mlawer, E., S. Taubman, P. Brown, M. Iacono, and S. Clough, 1997: Radiative transfer for inhomogeneous atmosphere: RRTM, a validated correlated-*k* model for longwave. *J. Geophys. Res.,* **102,** 16 663–16 682, doi:10.1029/97JD00237.

NWS, 1994: Excessive heat watch, warning and advisory heat index criteria. Regional Operations Manual Letter E-5-94, Eastern Region, National Weather Service, Bohemia, NY, 3 pp.

Oke, T. R., and R. D. Bornstein, 1981: Influence of pollution on urban climatology. *Adv. Environ. Soc. Eng.,* **2,** 171–202.

Roberts, M., T. R. Oke, C. S. B. Grimmond, and J. A. Voogt, 2006: Comparison of four methods to estimate urban heat storage. *J. Appl. Meteor. Climatol.,* **45,** 1766–1781, doi:10.1175/JAM2432.1.

Rotach, M. W., 1993: Turbulence close to a rough urban surface. *Bound.-Layer Meteor.,* **65,** 1–28, doi:10.1007/BF00708816.

Roulet, Y., A. Martilli, M. W. Rotach, and A. Clappier, 2005: Validation of an urban surface exchange parameterization for mesoscale models—1D case in a street canyon. *J. Appl. Meteor.,* **44,** 1484–1498, doi:10.1175/JAM2273.1.

Sailor, D. J., and M. Hart, 2006: An anthropogenic heating database for major U.S. cities. Preprints, *Sixth Symp. on the Urban Environment,* Atlanta, GA, Amer. Meteor. Soc., 5.6. [Available online at https://ams.confex.com/ams/pdfpapers/105377.pdf.]

Salamanca, F., and A. Martilli, 2010: A new building energy model coupled with an urban canopy parameterization for urban climate simulations—Part I. Formulation, verification and a sensitive analysis of the model. *Theor. Appl. Climatol.,* **99,** 331–344, doi:10.1007/s00704-009-0142-9.

——, ——, M. Tewari, and F. Chen, 2011: A study of the urban boundary layer using different urban parameterizations and high-resolution urban canopy parameters with WRF. *J. Appl. Meteor. Climatol.,* **50,** 1107–1128, doi:10.1175/2010JAMC2538.1.

——, ——, and C. Yague, 2012: A numerical study of the urban heat island over Madrid during the DESIREX (2008) campaign with WRF and evaluation of simple mitigation strategies. *Int. J. Climatol.,* **32,** 2372–2386, doi:10.1002/joc.3398.

Schuman, S. H., 1972: Patterns of urban heat-wave deaths and implications for prevention: Data from New York and St. Louis during June, 1966. *Environ. Res.,* **5,** 59–75, doi:10.1016/0013-9351(72)90020-5.

Skamarock, W. C., and Coauthors, 2008: A description of the Advanced Research WRF version 3. NCAR Tech. Note TN-475+STR, 113 pp.